Modeling of Molecular Weight Distribution in Ring-opening Polymerization of L,L-Lactide

*Yingchuan Yu†, Eric J. Fischer, Giuseppe Storti, Massimo Morbidelli**

Institute for Chemical and Bioengineering, Department of Chemistry and Applied Biosciences, Swiss Federal Institute of Technology (ETH), 8093 Zurich, Switzerland

massimo.morbidelli@chem.ethz.ch

Abstract

The molecular weight distributions of poly(lactic acid) produced by ring-opening polymerization of L,L-lactide in bulk melt are measured and compared with the ones predicted using a kinetic model accounting for reversible catalyst activation, reversible propagation, reversible chain transfer to co-catalyst and inter-molecular transesterification. The same values of the model parameters as evaluated in previous works are used without any adjustment, i.e. the model is used in fully predictive way. In order to calculate the complete molecular weight distribution, the model equations are solved through two different numerical methods, "direct integration" of the population balances at all values of chain length, and "fractionated moments", where the chains are artificially classified into two different categories depending upon the experienced reaction steps. The accuracy of the molecular weight distributions calculated in the latter case is evaluated by comparison with those computed by solving the model equations with the "direct integration" method. It is found that the "fractionated moments" method provides enough accuracy and much smaller computational effort, thus representing an optimal tool for most modeling applications. Finally, the model predictions are compared with the experimental molecular weight distributions measured experimentally in bulk melt at 130°C and various initial concentrations of catalyst and co-catalyst. The generally good agreement verified between model and experiment after correcting for peak broadening, represents a convincing confirmation of the model reliability.

†Current affiliation: Sulzer Chemtech Ltd, Polymer Technology, Process Technology, 8404 Winterthur, Switzerland

Introduction

Important side reactions during polyester production are the so-called redistribution reactions, such as alcoholysis, acidolysis, intramolecular (backbiting) and intermolecular (transesterification) ester-ester interchange.[1-3] These reactions are expected to be especially relevant in bulk melt processes and to affect the molecular weight of the final product. Namely, they broaden the chain length distribution and eventually drive it to the well-known most probable Schulz-Flory distribution, given long enough time of reaction. Such a random reorganization of monomer units affects also the chain composition and it may lead to significant changes of polymer viscosity and other average properties.[4]

In the case of step-growth polymerization, a few modeling studies focused on these specific reactions have been reported in the literature.[5-9] Notably, Hermans[6] was the first one to report the detailed population balance equations for the end-group interchange reaction and to derive an approximate analytical solution for the chain length distribution. Lertola[8] solved numerically the detailed population balance equations using a direct integration method, i.e. solving all the balances for each value of chain length up to a maximum. This way, the complete discrete molecular weight distribution could be calculated. Tobita and Ohtani[9] solved again the population balances accounting for chain growth and redistribution through the method of moments. The resulting closure problem was solved in an approximate way, using a formula valid at limited extent of redistribution only. Notably, the model predictions were calculated with experimental results but only in terms of average properties, not of complete distributions. Finally, Jo et al.[7] applied Monte Carlo simulation to analyze the effect of redistribution reactions on molecular weight, confirming the approach to the most probable distribution starting from different, non-equilibrium distributions.

In ring-opening polymerization systems, and in particular for lactide polymerization carried out with catalysts, intermolecular interchange is the dominant redistribution process and the corresponding mechanism and kinetics have been reviewed by Duda and Penczek.[10, 11] It can be generically sketched as follows:

$$P_n + P_m \longrightarrow P_p + P_{n+m-p}$$

where P_j is the concentration of the active chains with j repeating units. Using such a reaction schematization together with reversible propagation, Szymanski[12] solved the resulting population balances using the Monte Carlo method and a so-called "approximate numerical method". In the latter case, the polymer chains were divided into two different classes, one including all the chains which never experienced transesterification and the other including all the remaining ones, i.e. those transesterified. The population balances of both types of chains were then separately written and numerically solved by the method of moments. The corresponding chain length distributions were finally estimated through a presumed model distribution tuned based on the calculated moments of the first three orders. This approach was demonstrated to be very effective to predict the complete molecular weight distribution with much less computational effort than in the Monte Carlo case. On the other hand, Szymanski[12] solved the population balances considering lactide as repeating unit, while lactoyl unit should be considered to account properly for transesterification reactions. This way, potential sites for chain exchange were neglected, thus affecting calculated results as well as corresponding parameter values. Moreover, the kinetic scheme was quite simplified and no comparison with experimental data was attempted.

In this work, the simulation of the ring-opening polymerization of lactide is once more examined considering a comprehensive kinetic scheme involving reversible

catalyst activation, reversible propagation, reversible chain transfer and inter-molecular transesterification. Such a kinetic scheme has been recently applied and validated for the ROP of L,L-lactide.[13, 14] Two numerical methods are applied to the resulting set of model equations: first, all the population balances are individually solved for each chain length up to a suitable maximum value. This method is defined "direct integration" and provides the most accurate results; therefore, its solution will be considered as the reference one. Second, a modified version of the "fractionated moments" method proposed by Szymanski[12] is developed and validated by comparison with the results provided by the first method. Finally, once proven the reliability of the predictions offered by the second method as well as its limited computational effort, a comparison of its predictions to experimental data of ROP of L,L-lactide in bulk melt is carried out. Namely, the calculated molecular weight distributions are compared with those measured by size exclusion chromatography (GPC) at different reaction conditions. It is well known that the imperfect resolution of GPC leads to the band broadening effect on the experimental determined molecular weight distribution.[15] Thus, the comparison has been performed after applying a suitable correction to introduce the spurious axial-mixing effects in the calculated molecular weight distributions.

Experimental Part

Materials. (S,S)-3,6-Dimethyl-1,4-dioxane-2,5-dione (L,L-Lactide; PURAC, ≥99.5% GC, water: <0.02%, free acid: <1 meq kg^{-1}) was further recrystallized in toluene (Sigma-Aldrich, puriss. p.a., ≥99.7% GC, H_2O <0.001%). 2-ethylhexanoic acid tin(II) salt ($Sn(Oct)_2$; Sigma Aldrich, 95% purity), 1-dodecanol (Fluka, 99.5% purity), lactic acid anhydrous (ABCR Chemicals, Karlsruhe, 99% purity), toluene

anhydrous were used to facilitate catalyst transfer (99.8%, packaged under Argon), Polystyrene standards from 500 Da to 2,000,000 Da (Sigma Aldrich) were used for calibration and Chloroform (J. T. Baker) as eluent.

Reaction Procedure. L,L-Lactide (LA) was melted at temperature below 100°C in a stirred flask in glove box and then catalyst (stannous octoate) and co-catalyst (lactic acid anhydrous) were dissolved in anhydrous toluene (10 wt%) in glove box at given molar ratio with respect to monomer. Anhydrous toluene was used to facilitate the transfer of catalyst and co-catalyst to the mother flask without contaminations. The free acids were added directly into the flask at given ratios with respect to the catalyst. The final mixtures were transferred to glass vials and sealed with T-type poly(tetrafluoroethylene) caps in order to prevent the loss of LA during the reaction by vaporization and recrystallization. All vials were finally transferred into a controlled heating block kept at constant temperature (130 ± 1°C). The final product in the different reaction vials was finally quenched in an ice bath at different times and kept in refrigerator for further characterizations. Reactions at constant amount of catalyst, co-catalyst and different amounts of free acid have been carried out.

MALDI-TOF Mass Spectrometry. MALDI TOF Mass Spectra were measured by an Ultraflex II TOF Bruker spectrometer (Bremen, Germany) using 2-[(2E)-3-(4-tert-Butylphenyl)-2-methylprop-2-enylidene]malononitrile (DCTB) as matrix material. Samples co-crystallized with the matrix on the probe were ionized by Smart Bean laser pulse (337 nm) and accelerated under 25 kV with time-delayed extraction before entering the time-of-flight mass spectrometer. Matrix (DCTB) and sample were separately dissolved in dichloromethane and mixed in a matrix to sample ratio of 10:1. To produce some special adducts, sodium ions are added (1% sodium acetate in methanol). 1 μL mixture of matrix and sample was applied to a MALDI-TOF MS

probe and air dried. All spectra were performed in positive reflection mode. External calibration was performed by using peptide calibration standard II (700 Da - 3200 Da), protein calibration standard I (5000 Da – 17000 Da) and protein calibration standard II (20000 Da – 50000 Da) from Care (Bruker).

GPC Analysis. Conversion and molecular weight distribution of all samples were characterized by Size Exclusion Chromatography (GPC) (Agilent, 1100 series) equipped with two detectors, Ultraviolet and Differential Refractive Index. Depending upon the molecular weight of the specific sample, pre-column and oligopore column (Polymer Laboratories, length of 300 mm and diameter of 7.5 mm, measuring range 0 – 4,500 Da) or pre–column and two PLgel 5 μm MIXED–C columns (Polymer Laboratories, length of 300 mm and diameter of 7.5 mm, measuring range 2,000 – 2,000,000 Da) have been used. Chloroform was used as eluent at flow rate of 1 mL min^{-1} and temperature of 30°C. Universal calibration was applied, based on poly(styrene) standards and the following equation:[16]

$$\ln M_2 = \frac{1+a_1}{1+a_2}\ln M_1 + \frac{1}{1+a_2}\ln\left(\frac{K_1}{K_2}\right) \quad (1)$$

where *a* and *K* are the Mark–Houwink constants for PLA (index 2) and the reference polymer (index 1), respectively. The following values of the Mark–Houwink constants have been used in this work: for PLLA,[17] K_2 = 0.01709 mL g^{-1} and a_2 = 0.806; for poly(styrene): K_1 = 0.0049 mL g^{-1} and a_1 = 0.794.[18]

Model Development

The kinetic scheme of the catalytic ROP of L,L-lactide is shown in Scheme 1.[13, 14] It involves reversible catalyst activation (a), reversible propagation (b), reversible chain transfer (c), inter-molecular transesterifications between two active chains (d) and

between active and dormant chains (e). Note that all examined experiments have been carried out at 130 °C. At this temperature, thermal degradation, also referred to non-radical random chain scission,[14] is negligible and, therefore, it was excluded from the kinetic scheme.

(a) $C + D_n \underset{k_{a2}}{\overset{k_{a1}}{\rightleftarrows}} R_n + A$

(b) $R_n + M \underset{k_d}{\overset{k_p}{\rightleftarrows}} R_{n+2}$

(c) $R_n + D_m \underset{k_s}{\overset{k_s}{\rightleftarrows}} D_n + R_m$

(d) $R_n + R_m \underset{k_{ts}}{\overset{k_{ts}}{\rightleftarrows}} R_{n+m-j} + R_j$

(e) $R_n + D_m \underset{k_{ts}}{\overset{k_{ts}}{\rightleftarrows}} R_{n+m-j} + D_j$

Scheme 1. Kinetic scheme of ROP of L,L-lactide at 130°C. (a) reversible catalyst activation, (b) reversible propagation, (c) reversible chain transfer, (d) and (e) inter-molecular transesterification.

In the specific case under examination (tin(II) 2-ethylhexanoate (stannous octoate, $Sn(Oct)_2$) as catalyst and 1-dodecanol as co-catalyst), the symbols used in the previous scheme correspond to the following chemical species: C = $Sn(Oct)_2$, A = OctH, M = $C_6H_8O_4$, R_0 = -SnOR, R_n = -$SnO(LA)_nR$, D_0 = HOR, and D_n = $HO(LA)_nR$. Moreover, LA is the repeating lactoyl unit ($C_3H_4O_2$) and R = $C_{12}H_{25}$. According to the selected schematization, the catalyst can be activated by any species bearing a hydroxyl end group (the co-catalyst or any dormant chain) to form an active chain with octanoic acid as side product. The resulting active chain then propagates by monomer addition (note that each unit of lactide contributes with two lactoyl repeating units[14]). Meanwhile, the active chain can also react with a dormant species to form an active as well as a dormant chain with different chain lengths: this reaction is the so called reversible chain transfer. Catalyst activation and chain transfer

reactions are fast enough to become practically instantaneous: then, all active and dormant chains are formed at the very beginning of the polymerization and remain in constant amount all along the reaction, as typical of living polymerizations.[19, 20] Finally, the inter-molecular transesterifications (d) and (e) are considered. These reactions become dominant at high conversion, usually larger than 90%.[13] However, their effect on the molecular weight distribution is significant all along the reaction. In the presence of a catalyst, all ester bonds can be transesterified: then, any polymer chain may undergo the chain reshuffling process. To better illustrate the impact of such reactions on the chain length, let us discuss the schematic representation in Scheme 2.

Let us focus on the consumption rate of active chains by transesterification: as shown in the scheme, an active chain with length *n* can be "consumed" by attacking any ester group in another active chain of length *j* (a) or being attacked by another active chain of any chain length (b). Let us now consider the rate of "formation" of the same type of active chains of length n. These can be formed by transesterification reactions in two ways: an active chain, whose length is shorter than *n* (let us say *m*), can attack any other active chain, and link a number of units so as to produce a new active chain with length n (c) or a chain of length larger than n is attacked by another active chain and releases an active chain with length *n* (d). According to the literature,[10, 11] any active chain is able to attack any other polymer chain (active or dormant) containing ester bonds, whereas a dormant chain can be only attacked by an active chain to undergo chain reshuffling. Then, the transesterification kinetic terms in the balances of the dormant species have to be adapted accordingly.

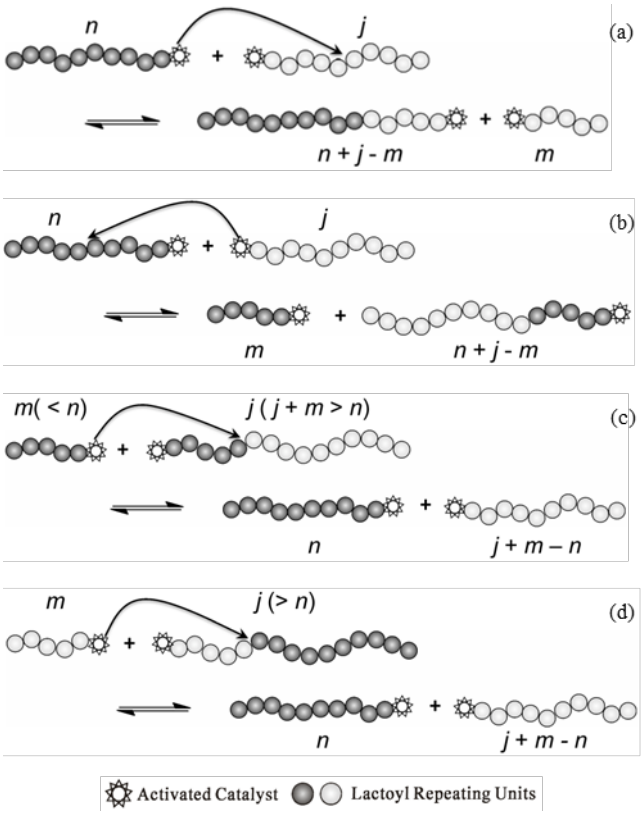

Scheme 2. Schematic illustration of inter-molecular transesterification reactions between active chains in ring-opening polymerization of L,L-lactide.

Given such schematization, the population balances can be written accounting for all the other typical reactions (catalyst activation, propagation and chain transfer) as shown below by Equations 5 and 6 for active and dormant chains, respectively. Along with the material balances of all the other species in the system (Equations 2 to 4), the developed kinetic model is made of the differential equations reported below:

$$\frac{dC}{dt} = -k_{a1} C \mu_0^D + k_{a2} A \mu_0^R \tag{2}$$

$$\frac{dA}{dt} = k_{a1} C \mu_0^D - k_{a2} A \mu_0^R \tag{3}$$

$$\frac{dM}{dt} = -k_p M \mu_0^R + k_d \left(\mu_0^R - R_1 - R_0 \right) \tag{4}$$

$$\begin{aligned}\frac{dR_n}{dt} &= k_{a1}CD_n - k_{a2}AR_n \\ &-k_pMR_n + k_dR_{n+2} + \left(1-\delta_{n,0}\right)\left(1-\delta_{n,1}\right)\left(k_pMR_{n-2} - k_dR_n\right) \\ &-k_sR_n\mu_0^D + k_sD_n\mu_0^R \\ &-k_{te}R_n\left(\mu_1^R - \mu_0^R + R_0 + \mu_1^D - \mu_0^D + D_0\right) \\ &-k_{te}\left(1-\delta_{n,0}\right)\left(1-\delta_{n,1}\right)\left(n-1\right)R_n\mu_0^R \\ &+k_{te}\left(1-\delta_{n,0}\right)\mu_0^R\sum_{i=n+1}^{\infty}\left(R_i + D_i\right) \\ &+k_{te}\left(1-\delta_{n,0}\right)\sum_{i=0}^{n-1}R_i\sum_{j=n-i+1}^{\infty}R_j\end{aligned} \tag{5}$$

$$\begin{aligned}\frac{dD_n}{dt} &= -k_{a1}CD_n + k_{a2}AR_n \\ &+k_sR_n\mu_0^D - k_sD_n\mu_0^R \\ &-k_{te}\left(1-\delta_{n,0}\right)\left(1-\delta_{n,1}\right)\left(n-1\right)D_n\mu_0^R \\ &+k_{te}\left(1-\delta_{n,0}\right)\sum_{i=0}^{n-1}R_i\sum_{j=n-i+1}^{\infty}D_j\end{aligned} \tag{6}$$

where the symbols μ_0^R and μ_0^D indicate the zero-th order moments of active and dormant chains, respectively, and $\delta_{n,j}$ is the Kronecker delta (equal to 1 when $n = j$ and zero otherwise). In the following, these equations have been solved using different methods; however, the same values of all model parameters have been used in all cases, as summarized in Table 1. These values have been found in the literature[13, 14, 20] for the ROP of L,L-lactide in bulk melt at 130°C and will be used without any adjustment.

Table 1. Numerical values of the model parameters at 130°C.[14]

Parameter	Symbol	Value
Reversible catalyst activation equilibrium constant	$K_{eq,a}$	0.045
Reversible catalyst activation rate coefficient	k_{a1}	10^6 L mol^{-1} h^{-1}

Reversible propagation rate coefficient	k_p	4500 L mol^{-1} h^{-1}
Monomer equilibrium concentration	M_{eq}	0.106 mol L^{-1}
Reversible chain transfer rate coefficients	k_{s1}, k_{s2}	10^6 L mol^{-1} h^{-1}
Inter-molecular transesterification rate coefficient	k_x	6 L mol^{-1} h^{-1}

Numerical solution

The first method applied to solve numerically the population balance equations above is the "direct integration" method. Each differential equation is solved directly for any value of *n* from 1 to a suitable maximum value. This approach clearly provides the most detailed solution but is very computationally intensive.

The second method is the so called "fractionated moments" method. As anticipated, it closely resembles the approach first introduced by Szymanski[12] in his "approximate solution", using a methodology conceptually equivalent to that previously introduced by Teymour and Campbell in their "numerical fractionation".[21] In short, the polymer chains are classified into several sub-groups so that a single, very heterogeneous group of polymer chains is represented as combination of several sub-groups each one more homogeneous. The fractionated populations are then solved numerically and the molecular weight distributions of each polymer group can be reconstructed from its first leading moments using standard numerical approaches.[22, 23] Such an approach works with sufficient accuracy provided that enough "homogeneity" has been achieved in the sub-groups when applying the selected fractionation rules. Following Szymanski, two groups only are enough, the first one including all chains that never experienced transesterification and the second all the others. Then, the concept behind

the success of the solution method is that the major differentiation into the polymer population is introduced by the first re-shuffling step.

The implementation of this method has been carried out by splitting the polymer chains into two categories, as shown in Equations 7 to 10. S_n and E_n indicate the concentrations of active and dormant chains which never underwent transesterification reactions, respectively, while T_n and F_n are active and dormant chains "produced" by transesterification. Of course, all types of chains are involved in all the reactions reported in Scheme 1: therefore, the concentrations of transesterified chains can be simply calculated by subtracting the non-transesterified chains from the total polymer chains calculated using the population balances 5 and 6. Accordingly, the relevant population balance equations are given by:

$$\begin{aligned}\frac{dS_n}{dt} &= k_{a1}CE_n - k_{a2}AS_n \\ &\quad -k_pMS_n + k_dS_{n+2} + \left(1-\delta_{n,0}\right)\left(1-\delta_{n,1}\right)\left(k_pMS_{n-2} - k_dS_n\right) \\ &\quad -k_sS_n\mu_0^D + k_sE_n\mu_0^R \\ &\quad -k_{te}S_n\left(\mu_1^R - \mu_0^R + R_0 + \mu_1^D - \mu_0^D + D_0\right) \\ &\quad -k_{te}\left(1-\delta_{n,0}\right)\left(1-\delta_{n,1}\right)\left(n-1\right)S_n\mu_0^R\end{aligned} \tag{7}$$

$$T_n = R_n - S_n \tag{8}$$

$$\begin{aligned}\frac{dE_n}{dt} &= -k_{a1}CE_n + k_{a2}AS_n \\ &\quad +k_sS_n\mu_0^D - k_sE_n\mu_0^R \\ &\quad -k_{te}\left(1-\delta_{n,0}\right)\left(1-\delta_{n,1}\right)\left(n-1\right)E_n\mu_0^R\end{aligned} \tag{9}$$

$$F_n = D_n - E_n \tag{10}$$

Since the above population balance equations, refer now to relatively homogeneous populations, a rather accurate numerical solution can be obtained using the method of moments. The resulting moment equations are summarized in the Appendix together

with the required closure formula.[23] Finally, the molecular weight distribution of each type of polymer chain sub-population is reconstructed using a modified Gamma distribution as model distribution[22]. This model distribution has been selected because it is monomodal and defined for positive values of the independent variable, like a generic molecular weight distribution. Then, the distribution of the whole polymer is then obtained by summing up the contributions of each sub-population. This overall distribution can then be compared to the one predicted by solving the population balances through the direct integration method or measured experimentally. More specifically, the molecular weight distribution of each polymer chain sub-population is evaluated as follows:[22, 23]

$$f(n) = \frac{b}{a}\, p^{(b)}\left(z\right)\lambda_0 \tag{11}$$

where n is the chain length, z a modified chain length ($z = b\ n\ /\ a$) and $p^{(b)}(n)$ the Gamma distribution defined as:

$$p^{(b)}(z) = \frac{1}{(b-1)!} z^{b-1} \exp(-z) \tag{12}$$

with a and b characteristic parameters evaluated as a function of the first three leading moments of the unknown distribution (μ_0, μ_1 and μ_2) and related to its shape and broadness as follows:

$$a = \mu_1 / \mu_0 \quad \text{and} \quad b = a^2 / (\mu_2 / \mu_0 - a^2) \tag{13}$$

Results and Discussion

Solution by the Direct Integration method. As mentioned above, with this method we compute the full molecular weight distribution of the polymer. Therefore, it is worth to compare the model predictions with the results provided by a very

detailed characterization technique such as MALDI-TOF. Both numerical solution and experimental technique provide in fact the concentration for every single value of the chain length, even though the quantitative reliability of the MALDI-TOF results is known to be limited to short chains (< 10,000 Da). Therefore, in Figure 1 we compare measured (a) and computed (b) chain length distributions at small enough monomer/catalyst ratio (PLA sample collected at 90% conversion during ROP in bulk melt at 130°C using crystalline lactic acid and stannous octoate as co-catalyst and catalyst, respectively, at OH_0/C_0 = 80 and M_0/C_0 = 1000). The peaks of both distributions are normalized by the maximum peak value and their corresponding *m/z* values represent the molecular weight of polymer with a specific chain length, where *m* and *z* are mass and charge of the specific macromolecules, respectively. Note that each lactide unit in the chain corresponds to two lactoyl repeating units while the co-catalyst, i.e. crystalline lactic acid, corresponds to one single repeating unit. Thus, without transesterification reactions, all PLA chains would be made of odd numbers of lactoyl repeating units. On the other hand, inter-molecular transesterification reshuffles the repeating units along the chains so that PLA chains with even numbers of lactoyl repeating units can be produced. This is confirmed by the experimental distribution shown in Figure 1(a): at conversion of 90%, most of the PLA chains have an odd number of repeating units, as indicated by the high intensity peaks in the distribution. However, significant fractions of chains with even numbers of repeating units are also present in the reaction system (low intensity peaks) and these are obviously the result of transesterification reactions. It is worth noticing that, since the transesterification is much slower than propagation, the fraction of even chains remains smaller than that of odd chains.

Let’s now consider the predictions of the model when solved by the direct integration method. At the same reaction conditions and using the parameter values in Table 1, the calculated results shown in Figure 1(b) are obtained. Note that the model provides the concentrations of the different polymer chains and not their intensities, as in the spectrum measured by MALDI-TOF. Thus, it is assumed that all calculated chain concentrations are proportional to the corresponding intensities and that the corresponding proportionality constants are independent upon the chain length. All the intensities, experimental and calculated, are then normalized in order to facilitate the comparison of two spectra; namely, all values have been divided by the maximal value of the entire set shown in the figure. Even though the predicted molecular distribution is not perfectly superimposed to the experimental one, it is almost identical in shape. And, most important, the model correctly predicts the nature of the detailed experimental distribution, where both even and odd chain length are present but with significantly different amounts. Such an agreement constitutes a convincing confirmation of the reliability of the selected kinetic scheme and, in particular, of the role of the exchange reactions.

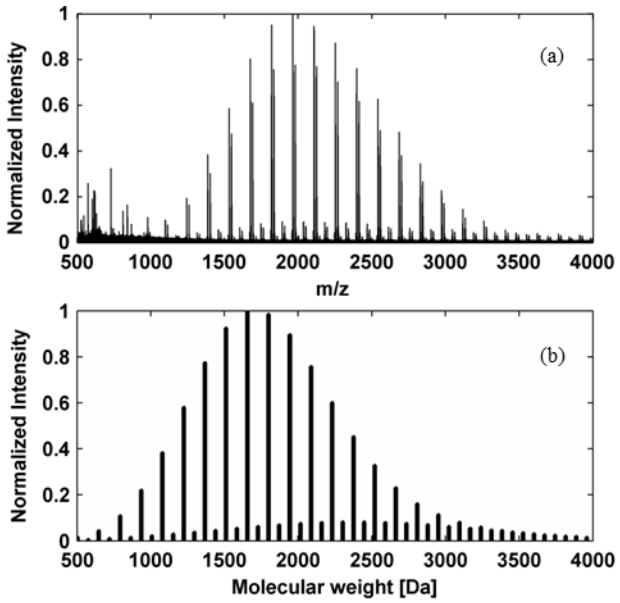

Figure 1. Molecular weight distribution of PLA produced by bulk ROP of L,L-lactide at 130°C at conversion of 90%. Catalyst: stannous octoate (C); co-catalyst: crystalline lactic acid (OH). OH_0/C_0 = 80, M_0/C_0 = 1000. (a) MALDI-TOF distribution; (b) Simulated distribution.

Solution by the Fractionated Moments method. To extend this analysis to longer chain lengths (e.g. 100,000 Da), we need to change both the numerical technique used for solving the population balance equations and the experimental technique. About the first one, we replace the direct integration method with the less computationally intensive fractionated moments method. As mentioned above, the polymer chains are fractionated in two classes, transesterified and non-transesterified chains. Within each class, two different species are considered, the living and the dormant chains. The first three leading moments of each type of polymer chains are evaluated to reconstruct the corresponding chain length distributions, and from these moments, the overall distribution is finally calculated by summation. Thus, including the material balance equations for the low molecular weight species as well as all moments equations for the chain length distribution, slightly more than twenty equations need to be solved, comparing to the hundreds of thousands equations which need to be integrated using

the direct integration method. Therefore, the fractionated moments approach is indeed effective to calculate the full molecular weight distribution of high molecular weight polymers with reasonable computational effort. In order to check the accuracy of this method, a comparison with the molecular weight distributions computed by solving the model through the direct integration method is shown in Figure 2 (reaction conditions are reported in the figure caption). For completeness, the results of the classical method of moments, i.e. without any fraction, are also shown in the same figure. Note that in this case, the complete distribution is estimated from the overall moments of the first three orders as done for each group of polymer chains in the case of the fractionated moments method.

At short reaction times (0.1 hour; Figure 2(a)), the non-transesterified PLA chains with even repeating units are dominant and the role of transesterification reactions is negligible. The solution obtained using the direct integration method provides the “true” chain length distribution, with odd and even chains as discussed above. The distributions obtained from the method of moments (overall or fractionated) are very similar and represent a kind of “average” distributions where the even-odd detail is missing. It is worth noticing that due to the negligible role of the transesterification reaction, the role of fractionation is also negligible.

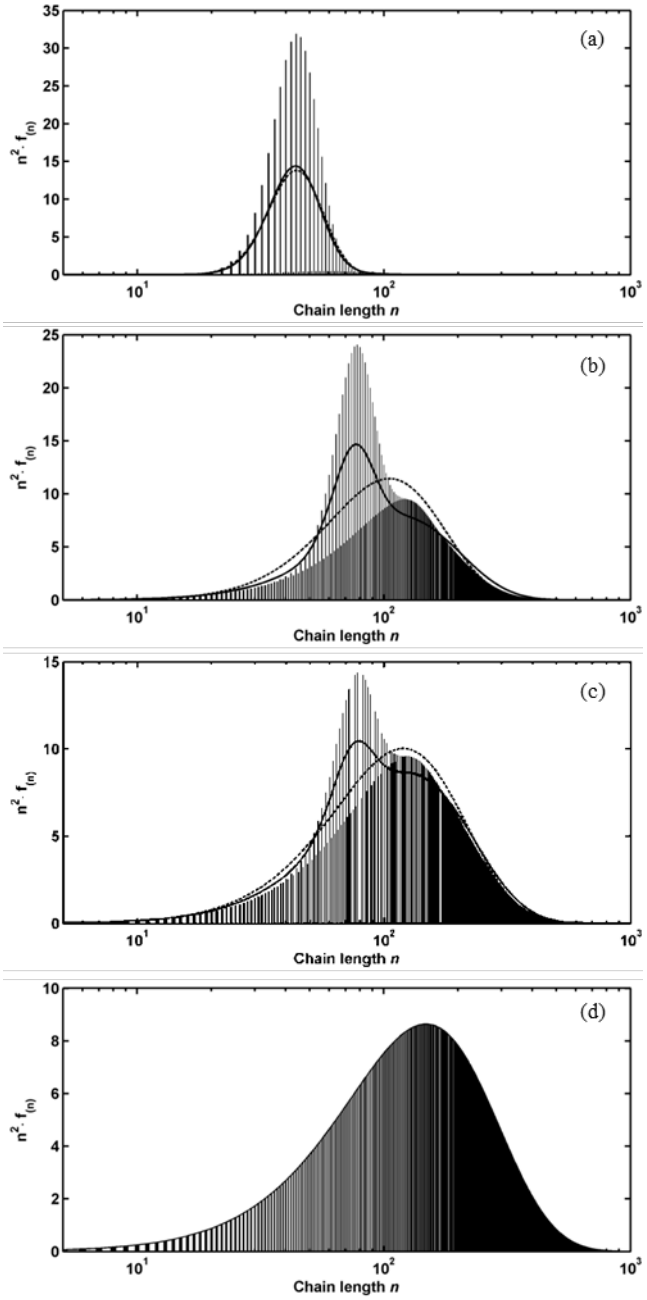

Figure 2. Calculated molecular weight distributions of the polymer produced by ROP of L,L-lactide in bulk melt at 130°C; OH_0/C_0 = 100; M_0/C_0 = 3771; reaction time: (a) = 0.1 h; (b) = 1 h; (c) = 1.5 h; (d) = 10h. Vertical bars: direct integration method; solid line: fractionated moments method; dashed line: moments method.

When the reaction time increases (1 hour; Figure 2 (b)), a clear bimodality arises in the distribution calculated with the direct integration method. The low molecular weight region represents non-transesterified chains and these are as usual indicated by

spikes of different heights for odd and even chains. On the other hand, these differences vanish at high molecular weight where transesterification reactions are dominant. As expected, the chain reshuffling process broadens the distribution and the range of chain lengths is significantly increased. It appears that the fractionated moments method also predicts the bimodality in the molecular weight distribution, although the detailed peaks corresponding to odd and even chain lengths are lost and the molecular weight distribution appears to be smooth also in the region of non transesterified chains. On the contrary, the bimodality is lost in the case of the conventional moment method, which is then proven to be fully inadequate.

At longer time, i.e. at 1.5 hours (Figure 2(c)), the non-transesterified chains are consumed by transesterification, so that the first peak in the figure decreases while the second one corresponding to transesterified chains becomes dominant. At reaction time of 10 hours (Figure 2(d)), all chains have experienced re-shuffling by transesterification and they are homogenous enough to fall into a monomodal chain length distribution. Accordingly, this can be nicely evaluated using their first leading moments only, without the need of any polymer fractionation: therefore, the three methods provide the same curves.

Summarizing, the direct integration method indeed predicts the fully detailed molecular weight distribution, whereas the fractionated moments method provides a kind of smooth interpolation of it. However, unlike the moments method without fractionation, the MWD bimodality predicted by solving the model equations through the “direct integration” method as well as the tailing effect at long reaction time (cf. Figure 2(c)) are correctly predicted. Now, two considerations need to be made: first, the computational effort is by far larger in the “direct integration” case than in the “fractionated moment” case. Second, when considering high molecular weights,

MALDI-TOF method cannot be used and we have to consider a different characterization method. Namely, we applied GPC: as it is well known, this is a chromatographic technique in which the sample flows through a packed column, thus experiencing different flow non-idealities such as axial or radial mixing.[15, 24-26] This leads to smoothed eluted peaks and reduces the "resolution" of the estimated distributions to a significant extent. Therefore, in order to make a fair comparison between experimental and model results, data treatment has been applied as detailed in the following.

Comparison with experimental data. In this section the model predicted distributions are compared with the experimental ones as measured by GPC for samples produced by ROP of L,L-lactide in bulk melt at 130°C. In all cases, the solution obtained through the fractionated moments method is considered. All the model parameter values have been used as reported in Table 1 without any adjustment.

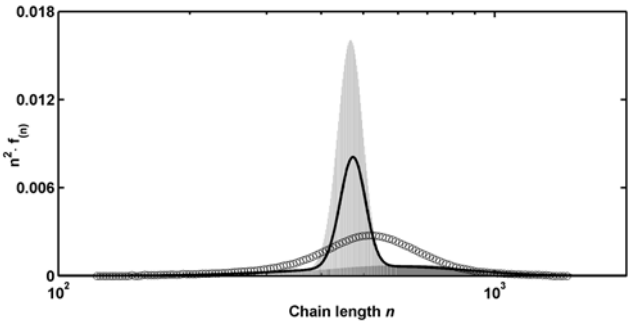

Figure 3. Comparison of experimental (○) and simulated distributions without accounting for axial mixing in the GPC measurement: direct integration (vertical bars); fractionated moments (solid line); $M_0 / C_0 = 1000$; $ROH_0 / C_0 = 2$; conversion at 47%.

The comparison is carried out in terms of chain weight distribution, $w(n) = n\, f(n)$, where $f(n)$ is the number distribution given by Equation 11. Moreover, in order to provide a convenient visualization of the distributions, $n \cdot w(n)$ is shown versus the degree of polymerization n (number of lactoyl units) using a logarithmic horizontal scale. This way, the area below each distribution is equal to the total number of lactoyl units in the polymer, thus proportional to its mass. All reported distributions have been normalized to their own first order moment.

The first comparison carried out between model and experiments is shown in Figure 3, where a clear disagreement is observed. All model predictions correspond to very narrow, sharp peaks which are not found experimentally using GPC. Such a disagreement can be due to spurious effects induced by the experimental characterization technique itself and, in particular, by flow non-idealities mentioned above. Therefore, the model predictions, which obviously are not affected by such phenomena, are expected to underestimate the experimental peak broadening, especially when they are very narrow. We therefore need to account for such axial mixing effects in order to prepare a fair comparison between simulation results and experimental data.

The effect of band broadening on GPC results has been subject of many literature contributions and a comprehensive review of different approaches has been recently published.[26] Among the different possibilities, we used the basic, "black-box" model proposed by Tung[25]; accordingly, the actually measured distribution, $F(v)$ – affected by axial mixing – is expressed as a broadened version of the "true" distribution, $W(y)$, by properly accounting for the symmetrical band broadening due to axial mixing as follows:

$$F(v) = \int_{v_a}^{v_b} W(y)\ g(v, y)\ dy \tag{14}$$

where v and y represent the elution volume and g is a suitable band broadening function. In particular, we adopted the following Gaussian-type expression:

$$g(v, y) = \sqrt{h/\pi}\ \exp[-h(v-y)^2] \tag{15}$$

where h is the resolution factor of the column, i.e. the parameter accounting for axial dispersion. Equation (14) has been applied with $W(y)$ equal to the distribution calculated by the model solved using the fractionated moments method, while the parameter h has been empirically estimated for the specific column we used. This was done by injecting a series of narrow poly(styrene) standards and fitting the resulting eluted peaks through the following version of Equation 14:

$$F(v) = A\ \sqrt{h/\pi}\ \exp[-h(v-v_p)^2] \tag{16}$$

where A is a constant related to the injected amount of poly(styrene) standard and v_p is the peak volume of the injected sample. Note that we assumed monodisperse standards, meaning that the entire broadening of the eluted peak was imputed to axial mixing only. A typical fitting of the eluted peak of a particular standard is shown in Figure 4(a); using standards with different molecular weights, the resolution factor was estimated as a function of molecular weight as shown in Figure 4(b). It is seen that in the range of molecular weight values of interest, i.e. from 4,000 to 700,000 Da, the resolution factor of the selected column is about 16.

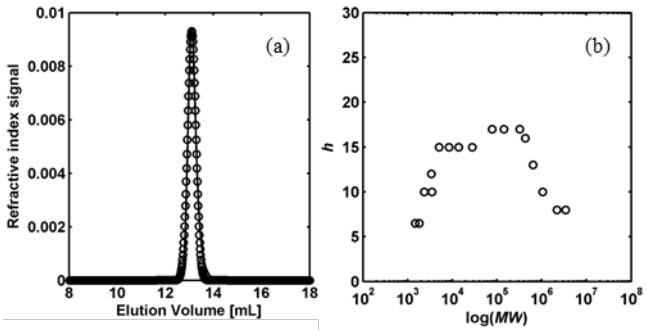

Figure 4. (a) Fitting of the GPC chromatogram measured by feeding a pulse of a poly(styrene) standard (M_p = 77,000 Da) using the Gaussian distribution (Eq. 15); (b) Resolution factor as a function of molecular weight of poly(styrene) standards.

Using Equation 14 to "correct" the model predictions in order to account for axial dispersion, we can finally compare the model predictions to the GPC chromatograms: such a comparison is shown in Figure 5. Four different samples at different values of conversion are considered for the following reaction conditions: bulk melt ROP of L,L-Lactide at 130°C; monomer to catalyst ratio, M_0 / C_0 = 3771; co-catalyst to catalyst ratio, ROH_0 / C_0 = 8. Note again that all simulations are genuinely predictive since no parameter adjustment was applied with respect to the values reported in Table 1 which have been estimated using independent experimental results not including the complete molecular weight distribution.[14]

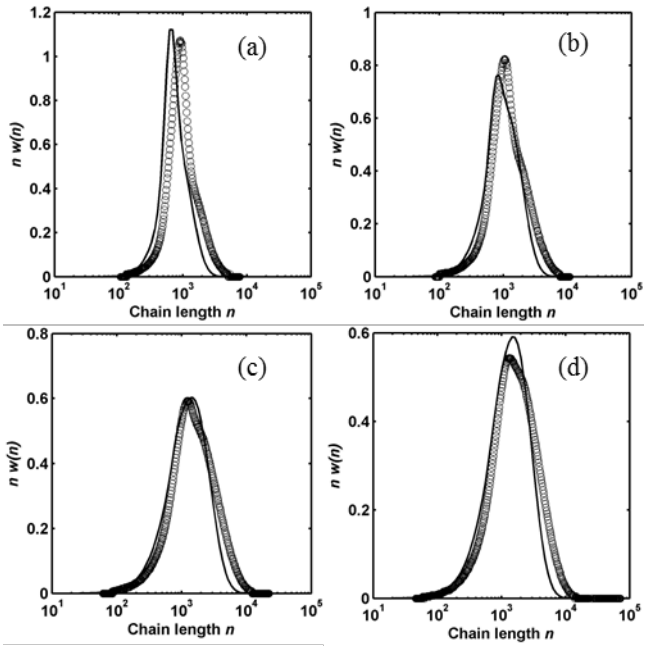

Figure 5. Comparison of experimental (empty circles) and simulated distributions (solid lines); M_0 / C_0 = 3771; ROH_0 / C_0 = 8; increasing conversion values: (a) = 68%; (b) = 81%; (c) = 91%; (d) = 93%.

The agreement between measured and predicted distributions is generally good. It can be seen that experimental distributions exhibit a shoulder at high molecular weights since the beginning of the reaction, which then tends to merge with the main peak as conversion increases. This shoulder represents in fact the fraction of transesterified chains and it is quite small at low conversion; however, its relevance increases at increasing conversion and eventually will absorb all the chains, as predicted by the model. At the reaction end, the distribution becomes monomodal, with dispersity value approaching the expected 2.

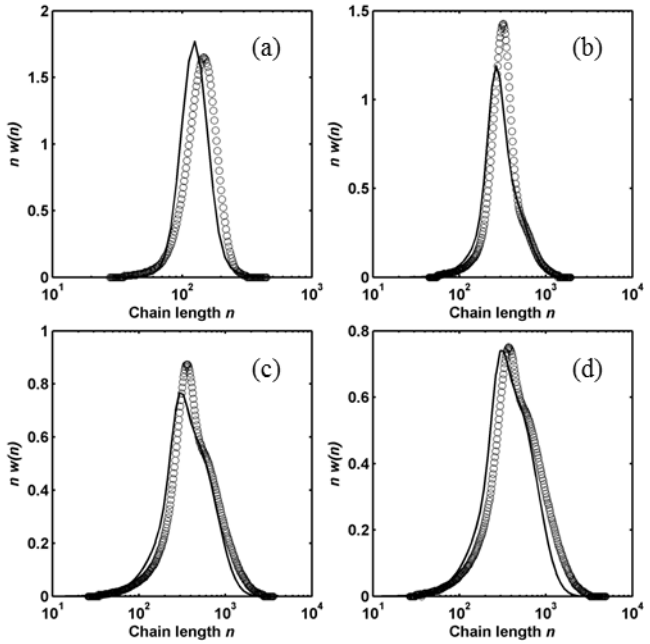

Figure 6. Comparison of experimental (empty circles) and simulated distributions (solid lines); M_0 / C_0 = 3771; ROH_0 / C_0 = 25; increasing conversion values: (a) = 41%; (b) = 92%; (c) = 95%; (d) = 96%.

The same comparison is shown in Figure 6 at larger co-catalyst amount (ROH_0 / C_0 = 25). The model predictions agree with the experimental results even better than in the previous case. The same bimodal behavior is found, with the narrow peak of the non-transesterified chains decreasing and the broad peak of the transesterified ones growing with conversion.

Finally, a reaction with larger catalyst content and small ratio co-catalyst/catalyst is examined (M_0 / C_0 = 1000, ROH_0 / C_0 = 2) in Figure 7. In this case, the relevance of transesterification reactions is expected to be comparable to that in Figure 5, due to the large amount of catalyst and the small ratio co-catalyst/catalyst. As in the previous cases, both the bimodal nature of the distributions and their conversion evolutions are nicely predicted.

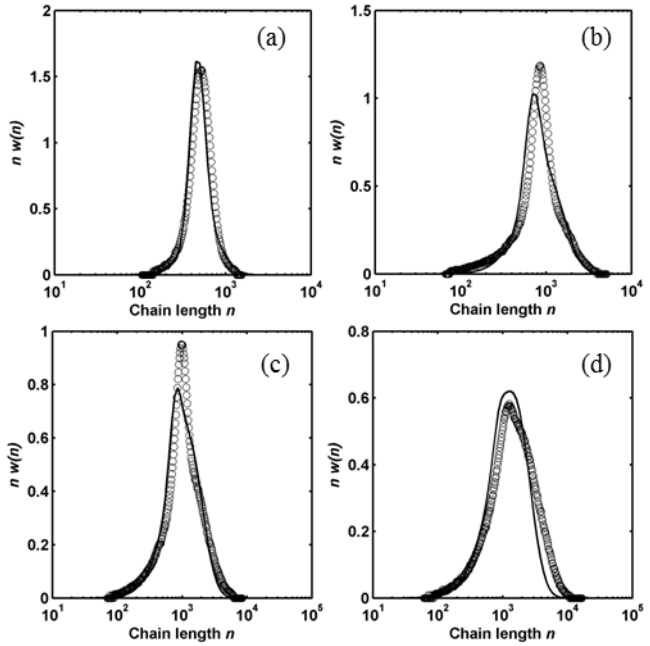

Figure 7. Comparison of experimental (solid lines) with simulated distributions (dashed lines); M_0 / C_0 = 1000; ROH_0 / C_0 = 2; increasing conversion values: (a) = 47%; (b) = 70%; (c) = 80%; (d) = 90%.

Conclusion

In this work, a previously proposed model of ROP of lactide[13, 14] has been numerically solved with the aim of predicting the complete molecular weight distribution of the polymer. The values of all model parameters have been used as estimated in a previous work[14] without any adjustment. Two different solution methods were applied and comparatively evaluated. The “direct integration” method provides the numerical reconstruction of the entire molecular weight distribution, but requires intensive computational effort. On the other hand, the “fractionated moments” method offers “smoothed” molecular weight distributions which are closer to those typically measured by GPC and it asks for much less computational time than the first method.

The predicted distributions calculated solving the model through the first method agree with the detailed picture provided by a characterization technique like MALDI-

TOF: the different amounts of chains with odd and even number of repeating lactoyl units are quite clear in both the experimental and calculated results, thus confirming the role of transesterification reactions. Moreover, comparing the solutions obtained using the two numerical methods, some loss of detail is apparent when looking at the distribution calculated using the "fractionated moments" method and focusing on the portion of the distribution where non-transesterified chains accumulate. On the other hand, the agreement between the distributions calculated using the two numerical methods becomes better and better at increasing reaction time, i.e. at increasing relevance of the transesterification reactions.

Finally, the simulation results obtained using the latter method, the one which best suites simulation of high molecular weight polymers, have been compared with experimental distributions measured by GPC. The time evolution of the molecular weight distribution, and in particular its bimodal nature, is well predicted. It is shown that such bimodality reflects the slow contribution of the transesterification reactions inside a kinetic scheme where different and faster reactions play a role in determining the final quality of the produced polymer.

Acknowledgment. The financial support provided by the Swiss Commission for Technology and Innovation (KTI/CTI; project no. 8611.2 PFIW-IW) is gratefully acknowledged.

Appendix

Moments definition

$$\mu_i^X = \sum_{n=0}^{\infty} n^i X_n \qquad (X = \text{R; S; T; D; E; F})$$

Moment equations

$$\frac{d\mu_0^R}{dt} = k_{a1} C \mu_0^D - k_{a2} A \mu_0^R$$

$$\begin{aligned}\frac{d\mu_0^S}{dt} &= k_{a1} C \mu_0^E - k_{a2} A \mu_0^S \\ &\quad - k_s \mu_0^S \mu_0^D + k_s \mu_0^E \mu_0^R \\ &\quad - k_{te} \mu_0^S \left(\mu_1^R - \mu_0^R + R_0 + \mu_1^D - \mu_0^D + D_0 \right) \\ &\quad - k_{te} \mu_0^R \left(\mu_1^S - \mu_0^S + S_0 \right)\end{aligned}$$

$$\frac{d\mu_0^D}{dt} = -k_{a1} C \mu_0^D + k_{a2} A \mu_0^R$$

$$\begin{aligned}\frac{d\mu_0^E}{dt} &= -k_{a1} C \mu_0^E + k_{a2} A \mu_0^S \\ &\quad + k_s \mu_0^S \mu_0^D - k_s \mu_0^E \mu_0^R \\ &\quad - k_{te} \mu_0^R \left(\mu_1^E - \mu_0^E + E_0 \right)\end{aligned}$$

$$\frac{d\mu_i^T}{dt} = \frac{d\mu_i^R}{dt} - \frac{d\mu_i^S}{dt}$$

$$\frac{d\mu_i^F}{dt} = \frac{d\mu_i^D}{dt} - \frac{d\mu_i^E}{dt}$$

$$\begin{aligned}\frac{d\mu_1^R}{dt} &= k_{a1} C \mu_1^D - k_{a2} A \mu_1^R \\ &\quad + 2k_p M \mu_0^R - 2k_d \left(\mu_0^R - R_1 - R_0 \right) \\ &\quad - k_s \mu_1^R \mu_0^D + k_s \mu_1^D \mu_0^R \\ &\quad - k_{te} \mu_1^R \left(\mu_1^D - \mu_0^D + D_0 \right) \\ &\quad + \frac{1}{2} k_{te} \mu_0^R \left(\mu_2^D - \mu_1^D \right)\end{aligned}$$

$$\frac{d\mu_1^S}{dt} = k_{a1}C\mu_1^E - k_{a2}A\mu_1^S$$
$$+2k_pM\mu_0^S - 2k_d\left(\mu_0^S - S_1 - S_0\right)$$
$$-k_s\mu_1^S\mu_0^D + k_s\mu_1^E\mu_0^R$$
$$-k_{te}\mu_1^S\left(\mu_1^R - \mu_0^R + R_0 + \mu_1^D - \mu_0^D + D_0\right)$$
$$-k_{te}\mu_0^R\left(\mu_2^S - \mu_1^S\right)$$

$$\frac{d\mu_1^D}{dt} = k_{a1}C\mu_1^D + k_{a2}A\mu_1^R$$
$$+k_s\mu_1^R\mu_0^D - k_s\mu_1^D\mu_0^R$$
$$-\frac{1}{2}k_{te}\mu_0^R\left(\mu_2^D - \mu_1^D\right)$$
$$+k_{te}\mu_1^R\left(\mu_1^D - \mu_0^D + D_0\right)$$

$$\frac{d\mu_1^E}{dt} = -k_{a1}C\mu_1^E + k_{a2}A\mu_1^S$$
$$+k_s\mu_1^S\mu_0^D - k_s\mu_1^E\mu_0^R$$
$$-k_{te}\mu_0^R\left(\mu_2^E - \mu_1^E\right)$$

$$\frac{d\mu_2^R}{dt} = k_{a1}C\mu_2^D - k_{a2}A\mu_2^R$$
$$+4k_pM\left(\mu_1^R + \mu_0^R\right) - 4k_d\left(\mu_1^R - \mu_0^R + R_0\right)$$
$$-k_s\mu_2^R\mu_0^D + k_s\mu_2^D\mu_0^R$$
$$-\frac{1}{3}k_{te}\mu_0^R\left(\mu_3^R - \mu_1^R\right)$$
$$-k_{te}\mu_2^R\left(\mu_1^D - \mu_0^D + D_0\right)$$
$$+k_{te}\mu_1^R\left(\mu_2^R - \mu_1^R\right)$$
$$+\frac{1}{6}k_{te}\mu_0^R\left(2\mu_3^D - 3\mu_2^D + \mu_1^D\right)$$

$$\frac{d\mu_2^S}{dt} = k_{a1}C\mu_2^E - k_{a2}A\mu_2^S$$
$$+4k_pM\left(\mu_1^S + \mu_0^S\right) - 4k_d\left(\mu_1^S - \mu_0^S + S_0\right)$$
$$-k_s\mu_2^S\mu_0^D + k_s\mu_2^E\mu_0^R$$
$$-k_{te}\mu_2^S\left(\mu_1^R - \mu_0^R + R_0 + \mu_1^D - \mu_0^D + D_0\right)$$
$$-k_{te}\mu_0^R\left(\mu_3^S - \mu_2^S\right)$$

$$\frac{d\mu_2^D}{dt} = -k_{a1}C\mu_2^D + k_{a2}A\mu_2^R + k_s\mu_2^R\mu_0^D - k_s\mu_2^D\mu_0^R + k_{te}\mu_2^R\left(\mu_1^D - \mu_0^D + D_0\right) + k_{te}\mu_1^R\left(\mu_2^D - \mu_1^D\right) + \frac{1}{6}k_{te}\mu_0^R\left(-4\mu_3^D + 3\mu_2^D + \mu_1^D\right)$$

$$\frac{d\mu_2^E}{dt} = -k_{a1}C\mu_2^E + k_{a2}A\mu_2^S + k_s\mu_2^S\mu_0^D - k_s\mu_2^E\mu_0^R - k_{te}\mu_0^R\left(\mu_3^E - \mu_2^E\right)$$

Closure formula

$$\mu_3 = \frac{\mu_2}{\mu_1\mu_0}(2\mu_0\mu_2 - \mu_1^2)$$

This formula is readily obtained following Hulburt and Katz[23]. Limiting ourselves to the evaluation of the moments of the first three orders (0, 1 and 2), any moment of different order *n* is estimated as:

$$\mu_n = \frac{(n+\lambda-1)!}{(\lambda-1)!}\frac{\mu_0}{(\lambda/a)^n}$$

where $\lambda = \frac{\mu_1^2}{\mu_2\mu_0 - \mu_1^2}$. For *n* = 3, the last previous equation reduces to the expression for μ_3 above.

References

(1) Flory, P. J. *Principles of Polymer Chemistry*. Cornell University Press: Ithaca, 1953.

(2) Hofman, A.; Slomkowski, S.; Penczek, S. Polymerization of Epsilon-Caprolactone with Kinetic Suppression of Macrocycles. *Makromol. Chem., Rapid Commun.* **1987**, *8*, 387.

(3) Kotliar, A. M. Interchange Reactions Involving Condensation Polymers. *J. Polym. Sci., Part D: Macromol. Rev.* **1981**, *16*, 367.

(4) Ramjit, H. G. The Influence of Stereochemical Structure on the Kinetics and Mechanism of Ester-Ester Exchange-Reactions by Mass-Spectrometry. II. *J. Macromol. Sci., Chem.* **1983**, *20*, 659.

(5) Abraham, W. H. Flory-Schulz Distribution in Reversible Semi-Batch Polycondensation. *Chem. Eng. Sci.* **1970**, *25*, 331.

(6) Hermans, J. J. Chain Length Distribution in a Polymer in Which Chain Ends React at Random with All Monomer Units. *J. Polym. Sci., Part C: Polym. Symp.* **1966**, *12*, 345.

(7) Jo, W. H.; Lee, J. W.; Lee, M. S.; Kim, C. Y. Effect of Interchange Reactions on the Molecular Weight Distribution of Poly(ethylene terephthalate): A Monte Carlo Simulation. *J. Polym. Sci., Part B: Polym. Phys.* **1996**, *34*, 725.

(8) Lertola, J. G. The Effect of Direct Interchange Reactions on the MWD of Condensation Polymers. *J. Polym. Sci., Part A: Polym. Chem.* **1990**, *28*, 2793.

(9) Tobita, H.; Ohtani, Y. Control of Molecular-Weight Distribution in Step-Growth Polymerization by an Intermediate Monomer Feed Method - Effect of Interchange Reactions. *Polymer* **1992**, *33*, 2194.

(10) Duda, A.; Penczek, S. *Biopolymers, Volume 3b, Polyesters II - Properties and Chemical Synthesis*, Wiley-VCH: Weinheim, 2002.

(11) Penczek, S.; Duda, A.; Szymanski, R. Intra- and Intermolecular Chain Transfer to Macromolecules with Chain Scission. The Case of Cyclic Esters. *Macromol. Symp.* **1998**, *132*, 441.

(12) Szymanski, R. Molecular Weight Distribution in Living Polymerization Proceeding with Reshuffling of Polymer Segments Due to Chain Transfer to Polymer with Chain Scission, 1 - Determination of k(p)/k(tr) Ratio from DP_w/DP_n Data. Ideal Reproduction of Polymer Chain Activities. *Macromol. Theory Simul.* **1998**, *7*, 27.

(13) Yu, Y. C.; Storti, G.; Morbidelli, M. Ring-Opening Polymerization of L,L-Lactide: Kinetic and Modeling Study. *Macromolecules* **2009**, *42*, 8187.

(14) Yu, Y. C.; Storti, G.; Morbidelli, M. Kinetics of Ring-Opening Polymerization of L,L-Lactide. *Ind. Eng. Chem. Res.* **2011**, *50*, 7927.

(15) Duerksen, J. H. Comparison of Different Techniques of Correcting for Band Broadening in GPC. *Sep. Sci.* **1970**, *5*, 317.

(16) Rudin, A. *Elements of Polymer Science and Engineering : An Introductory Text and Reference for Engineers and Chemists*; Academic Press: San Diego, 1999.

(17) Dorgan, J. R.; Janzen, J.; Knauss, D. M.; Hait, S. B.; Limoges, B. R.; Hutchinson, M. H. Fundamental Solution and Single-Chain Properties of Polylactides. *J. Polym. Sci., Part B: Polym. Phys.* **2005**, *43*, 3100.

(18) Kurata, M.; Tsunashima, Y. *Polymer Handbook*; Wiley-Interscience: New York, 1999.

(19) Kowalski, A.; Duda, A.; Penczek, S. Kinetics and Mechanism of Cyclic Esters Polymerization Initiated with Tin(II) Octoate. 3. Polymerization of L,L-dilactide. *Macromolecules* **2000**, *33*, 7359.

(20) Witzke, D. R.; Narayan, R.; Kolstad, J. J. Reversible Kinetics and Thermodynamics of the Homopolymerization of L-Lactide with 2-Ethylhexanoic Acid Tin(II) Salt. *Macromolecules* **1997**, *30*, 7075.

(21) Teymour, F.; Campbell, J. D. Analysis of the Dynamics of Gelation in Polymerization Reactors Using the Numerical Fractionation Technique. *Macromolecules* **1994**, *27*, 2460.

(22) Bamford, C. H.; Tompa, H. The Calculation of Molecular Weight Distributions from Kinetic Schemes. *Trans. Faraday Soc.* **1954**, *50*, 1097.

(23) Hulburt, H. M.; Katz, S. Some Problems in Particle Technology - a Statistical Mechanical Formulation. *Chem. Eng. Sci.* **1964**, *19*, 555.

(24) Balke, S. T.; Hamielec, A. E. Polymer Reactors and Molecular Weight Distribution .8. A Method of Interpreting Skewed GPC Chromatograms. *J. Appl. Polym. Sci.* **1969**, *13*, 1381.

(25) Tung, L. H. Method of Calculating Molecular Weight Distribution Function from Gel Permeation Chromatograms. *J. Appl. Polym. Sci.* **1966**, *10*, 375.

(26) Meira, G.; Netopilik, M.; Potschka, M.; Schnoll-Bitai, I.; Vega, J. Band Broadening Function in Size Exclusion Chromatography of Polymers: Review of Some Recent Developments. *Macromol. Symp.* **2007**, *258*, 186.

For Table of Contents use only

Modeling of Molecular Weight Distribution in

Ring-opening Polymerization of L,L-Lactide

Yingchuan Yu, Eric J. Fischer, Giuseppe Storti, Massimo Morbidelli